Additive Manufacturing 13 (2017) 61–70

Contents lists available at ScienceDirect

Additive Manufacturing

journal homepage: www.elsevier.com/locate/addma

Full length article

Effect of building direction on the microstructure and tensile properties of Ti-48Al-2Cr-2Nb alloy additively manufactured by electron beam melting

Mitsuharu Todai[a], Takayoshi Nakano[a,*], Tianqi Liu[a], Hiroyuki Y. Yasuda[a], Koji Hagihara[b], Ken Cho[a], Minoru Ueda[c], Masao Takeyama[d]

[a] Division of Materials and Manufacturing Science, Graduate School of Engineering, Osaka University, 2-1 Yamadaoka, Suita, Osaka 565-0871, Japan
[b] Department of Adaptive Machine Systems, Graduate School of Engineering, Osaka University, 2-1 Yamadaoka, Suita, Osaka 565-0871, Japan
[c] Metal Technology Co. Ltd., Harmony Tower 27F, 1-32-2 Honcho, Nakano-Ku, Tokyo 164-8721, Japan
[d] Department of Metallurgy and Ceramics Science, Tokyo Institute of Technology, 2-12-1 Ookayama, Meguro-ku, Tokyo 152-8550, Japan

ARTICLE INFO

Article history:
Received 7 July 2016
Received in revised form 26 October 2016
Accepted 7 November 2016
Available online 10 November 2016

Keywords:
Additive manufacturing
Electron beam melting (EBM)
Titanium aluminides
Tensile test
Microstructure

ABSTRACT

This paper clarified a novel strategy to improve the tensile properties of the Ti-48Al-2Cr-2Nb alloys fabricated by electron beam melting (EBM), via the finding of the development of unique layered microstructure composed of duplex-like fine grains layers and coarser γ grains layers. It was clarified that the mechanical properties of the alloy fabricated by EBM can be controlled by varying an angle θ between EBM-building directions and stress loading direction. At room temperature, the yield strength exhibits high values more than 550 MPa at all the loading orientations investigated ($\theta = 0$, 45 and 90°). In addition, the elongation at $\theta = 45°$ was surprisingly larger than 2%, owing to the development of this unique layered microstructure. The anisotropy of the yield strength decreased with increasing temperature. All the examined alloys exhibited a brittle-ductile transition temperature of approximately 750 °C and the yield strength and tensile elongation at 800 °C were over 350 MPa and 40%, respectively.

By the detailed observation of the microstructure, the formation mechanism of the unique layered microstructure was found to be closely related to the repeated local heat treatment effect during the EBM process, and thus its control is further possible by the tuning-up of the process parameters. The results demonstrate that the EBM process enables not only the fabrication of TiAl products with complex shape but also the control of the tensile properties associated with the peculiar microstructure formed during the process.

1. Introduction

TiAl-based alloys have been considered as potential candidates for aeroengine gas turbine applications because of their low density, high-temperature specific strength and superior corrosion resistance [1–3]. These alloys have already been used in commercial applications such as low-pressure turbine blades on current turbine engines and turbochargers for automobiles [4]. However, the poor room temperature ductility and high reactivity of TiAl alloys make them difficult to process and limit their application [5]. To overcome these disadvantages, a powder-bed additive manufacturing (AM) process [6,7] has emerged as a promising fabrication process for TiAl alloys [8–16]. Powder-bed AM process offers advantages in terms of reduced material waste, ability to create complex shape and a decrease in lead time. The process steps are as follows: (i) one layer of metal powder is selectively melted and solidified by energy source scanning based on two-dimensional slice data that is converted from three-dimensional (3D) computer-aided design data; (ii) The starting plate is lowered by one layer thickness; (iii) the rake feeds a new metal powder layer; (iv) the above process is repeated to produce a 3D structure. The powder layer is melted by either an electron beam or a laser as the energy source during the powder-bed AM process. Electron beam melting (EBM) has been receiving considerable attention because it realizes near-net-shape fabrication of TiAl alloys with low residual stress, compared with selective laser melting (SLM) [8–16]. Thus, several studies have been carried out to fabricate TiAl alloys by EBM [8–13]. Cormier et al. [8] and Murr et al. [9] characterized the microstructure of pre-

* Corresponding author.
E-mail address: nakano@mat.eng.osaka-u.ac.jp (T. Nakano).

http://dx.doi.org/10.1016/j.addma.2016.11.001

cursor powder and fabricated samples of TiAl alloys by EBM. They also reported the potential to fabricate TiAl products with complex shape using EBM. Schwerdtfeger et al. [10] reported on a process window for processing Ti-48Al-2Cr-2Nb (at%) alloy and the effect of the process parameters on the chemical composition [10]. Biamino et al. [11] reported the microstructure homogeneity of as-EBM specimen and the effect of both heat treatment and hot isostatic pressing (HIP) on the microstructure and mechanical properties of Ti-48Al-2Cr-2Nb alloys. Despite the success in the fabrication of TiAl alloys, the mechanical properties of as-EBM specimens need to be further improved for aerospace applications. In particular, the poor ductility of as-EBM specimens at ambient temperature should be overcome, for industrial applications, while ensuring sufficient strength, creep resistance and fracture toughness [1–3].

It is well known that the mechanical properties of TiAl alloys are significantly affected by the microstructure, which can be sensitively changed by heat-treatment [1–3]; it is generally considered that a fine equiaxed microstructure is preferable for ductility and strength, while a coarser full-lamellar microstructure (or near-lamellar) is preferable for creep properties. Thus, one approach for improving the mechanical properties of as-EBM TiAl alloys is to control the microstructure. Control of the microstructure and crystallographic texture by EBM and SLM processes has been examined in other alloys such as Ti–6Al–4 V alloys [17–19], stainless steels [20], Ni–based alloys [21] and Co–Cr alloys [22]. It was also reported that the microstructure of TiAl alloys fabricated by EBM was sensitive to the process parameters [10,13], but the details are not sufficiently clarified yet. During EBM, the electron beam locally melts successive layers of powder to produce TiAl alloy parts, accompanied by the local heat treatment in the vicinity around the melting pool. Thus, there is a possibility that the control of microstructure which is composed of suitable arrangement of different microstructural layers is achieved by EBM. However, such control of the microstructure in TiAl alloys focusing on local heat treatment under the melting layer during the EBM process has not been sufficiently explored. It is also well known that Ti-48Al-2Cr-2Nb alloys exhibit good oxidation resistance and a relatively good balance of mechanical properties up to 750 °C [3,23,24]. Therefore, the purpose of the present study is to control the microstructure of a Ti-48Al-2Cr-2Nb alloy by EBM. As a result, we found the development of unique layered microstructure. The influence of the development such unique microstructure on the tensile properties of as-EBM specimens was investigated.

2. Material and methods

The EBM specimens were fabricated using an Arcam A2X EBM system (Arcam AB, Mölndal, Sweden). The precursor powder of the Ti-48Al-2Cr-2Nb alloy, used in the present study, consists of spherical particles of which average diameter is around 100 μm. An electron beam was scanned according to a zigzag pattern; the building path was rotated by 90° between each layer. The cylindrical bars of Ti-48Al-2Cr-2Nb alloy were fabricated by EBM operated at 60 kV. The layer thickness for each fed powder layer was 90 μm and the pre-heating temperature before melting powder layer was 1060 °C. The angle (θ) between the building direction and cylindrical axis of these rods was set to 0°, 45° and 90°, as shown in Fig. 1. The constituent phases in as-EBM specimens were identified by X-ray diffraction analysis (XRD, Philips X-pert Pro). Specimens for the microstructure observation were cut from the as-EBM bars by electro-discharge machining and were subsequently polished mechanically and electrolytically in a perchloric acid: butanol: methanol solution (6: 35: 59 vol%) to remove the surface damage. The microstructures were examined using an optical microscope (OM) and a scanning electron microscope (SEM, JEOL JSM-6500F).

Table 1
Chemical composition of the as-received powder and the as-EBM specimen at $\theta = 0°$ in at% and wt% units.

	Elemental chemical composition						
	Ti	Al	Cr	Nb	C	O	N
(at.%)							
Powder as received	Bal.	48.6	1.74	1.95	0.032	0.193	0.008
Specimen as EBM	Bal.	46.3	1.72	2.10	0.049	0.215	0.020
(wt.%)							
Powder as received	Bal.	34.0	2.34	4.69	0.010	0.080	0.003
Specimen as EBM	Bal.	31.9	2.28	4.99	0.015	0.088	0.007

Specimens were etched using a solution consisting of 2.5 mL of HF, 4.5 mL of HNO_3 and 250 mL of H_2O for the OM observations.

Tensile specimens were cut by electro-discharge machining from the center of the as-EBM bars. The dimensions of the tensile specimens were approximately 0.8 × 1.5 mm in cross section and 5 mm in gauge length. Note that the loading axis was set to be parallel to the cylindrical direction. Tensile tests were conducted in vacuum at various temperatures between room temperature and 800 °C at a nominal strain rate of $1.67 \times 10^{-4}\ s^{-1}$. The slip markings were observed using an OM equipped with Nomarski interference contrast. The deformation microstructure was observed using a transmission electron microscope (TEM, JEOL JEM- 3010) operated at 300 kV. Thin foils for TEM observations were prepared by electropolishing in an acidic electrolyte. In order to examine the mechanical properties of the local area, nanoindentation hardness was measured using a nanoindenter (Elionix, ENT-1100a) at a maximum load of 29.4 mN.

3. Results

3.1. Unique layered microstructure of Ti-48Al-2Cr-2Nb alloy fabricated by EBM

The chemical compositions of the precursor powder and $\theta = 0°$ specimen prepared by EBM are shown in Table 1. It is pointed out that contamination by impurities such as oxygen, nitrogen and carbon is very limited thanks to the high-vacuum environment in the Arcam A2X EBM system. This is very important because these impurities decrease the ductility of this alloy at room temperature [25]. In addition, the loss of Al during EBM, which is reported to be caused by the evaporation due to high temperature during the EBM [11,13], is approximately 2 at%. Fig. 2 shows the variation of the XRD profiles of the $\theta = 0°$, 45° and 90° specimens. Diffraction peaks for γ-TiAl and α_2-Ti_3Al phases are clearly visible, suggesting that the two-phase structure composed of the γ and α_2 phases was predominately produced in the alloys regardless of the θ. The γ phase is ideally the tetragonal structure ($L1_0$, P4/mmm, $a = 0.3997$ nm and $c = 0.4062$ nm for the Ti-50Al alloy) and the α_2 phase is the hexagonal structure ($D0_{19}$, $P6_3/mmc$, $a = 0.5765$ nm and $c = 0.4625$ nm for the Ti-25Al alloy) [3]. From the intensity ratio between the XRD peaks of the γ and α_2 phases, the volume factions of these phases are similar in these specimens. In Fig. 2, the peaks corresponding to the β phase with the body centered cubic (bcc) structure were also detected although the intensity is much weaker than those of the γ and α_2 phases. Microstructural observation using the electron backscatter diffraction pattern analysis in the scanning electron microscopy (SEM-EBSD), it was confirmed that the β phases exist mostly near the surface region in the fabricated samples where rapid solidification occurred, and it was hardly seen in the central part of the prepared samples where the mechanical properties were examined in the following sections.

Fig. 3 shows the microstructure in the cylindrical EBM-built bars as a function of θ. These micrographs were taken in the cross-

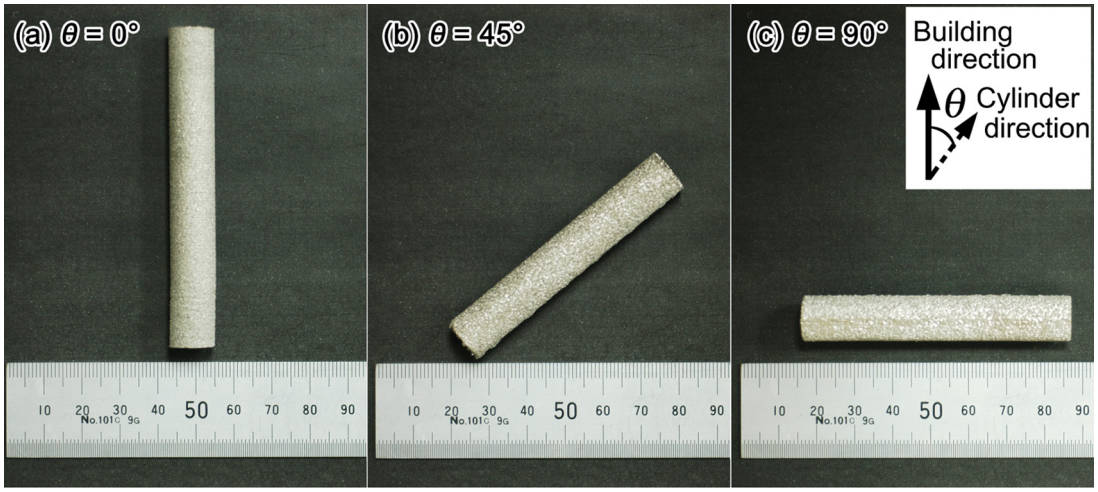

Fig. 1. Ti-48Al-2Cr-2Nb alloy specimens fabricated by EBM at $\theta = 0^\circ$ (a), $\theta = 45^\circ$ (b) and $\theta = 90^\circ$ (c).

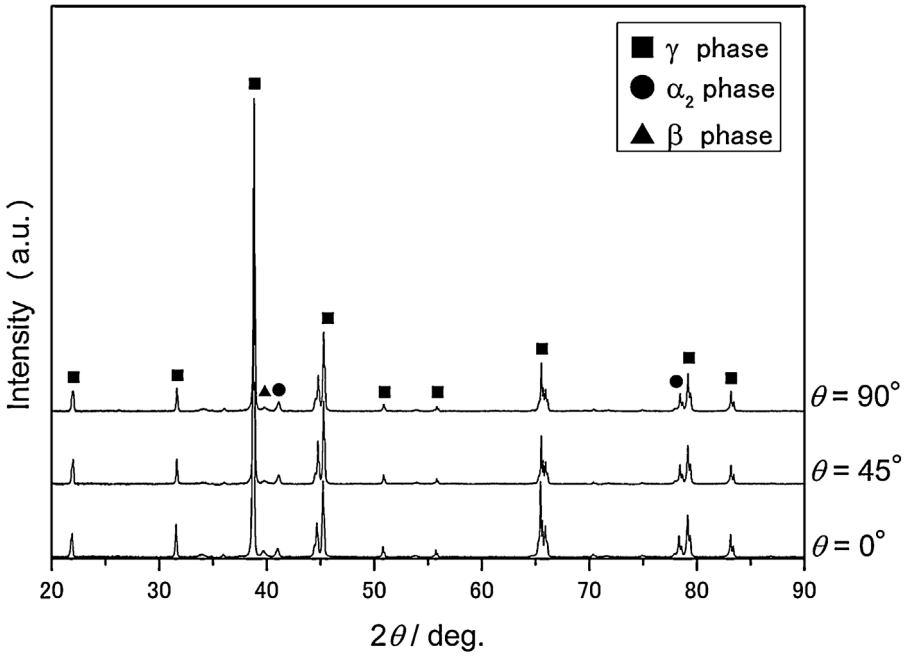

Fig. 2. XRD patterns of the vertical cross-section of $\theta = 0^\circ$, 45° and 90° specimens.

sections with respect to the building direction. Fig. 3(a)–(c) show low magnification micrographs of the specimens built at $\theta = 0^\circ$, 45° and 90°, respectively. Cracks due to thermal stress and residual pores are rarely observed in these specimens. In addition, the total porosity was determined to be less than 0.5% in all the examined specimens. This demonstrates that the process parameters of EBM in the present study can produce dense Ti-48Al-2Cr-2Nb alloy specimens. It is emphasized here that in Fig. 3 (a)–(c), some chains of equiaxed grains aligned perpendicular to the building direction can be seen. The observation in the high magnification images in Fig. 3(d)–(f) suggested that the microstructure is composed of the repeated stack of two layers with different characteristic features. One is predominantly composed of lamellar-structured γ/α_2 fine grains and fine equiaxed γ grains, and another is composed of coarser equiaxed γ phase grains which form a chain perpendicular to the building direction. These were further confirmed by the TEM observations, as described later. Hereafter, these two layers are referred to as duplex-like region and γ band region, respectively. In the γ bands, the α_2 phase is hardly observed. The layer thickness of the duplex-like region and the γ band region was measured along the building direction in the vertical cross-section, as shown in Fig. 3(g). The error bars in the figure correspond to the standard deviation of the thickness. Regardless of θ, the average layer thickness of the duplex-like region and the γ band was approximately 60 μm and 30 μm, respectively. It should be noted that the sum of these layer thicknesses corresponds approximately to the average thickness of powder layer fed at each cycle during the EBM process, suggesting that the formation of the unique layered microstructure shown in Fig. 3 is closely related to the layer-by-layer building. Fig. 3(h) shows the average grain size in the duplex-like region and the γ bands. When the average grain size in the duplex-like region was evaluated, the lamellar and γ grains were taken into consideration. As shown in Fig. 3(h), the average grain size is also independent of the angle θ. The grain size in the γ bands is approximately 20 μm, which is larger than that of the duplex-like region. The average grain sizes in as-EBM specimens are extremely small

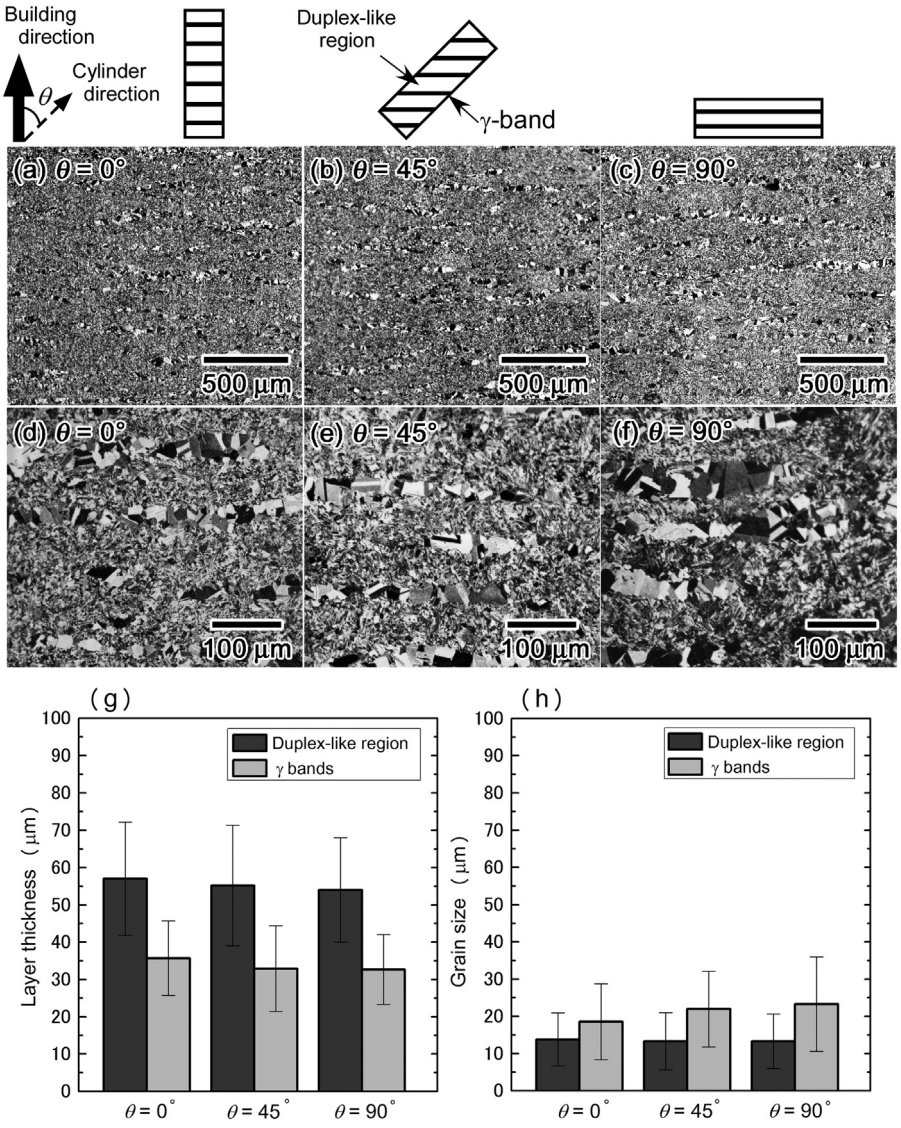

Fig. 3. Microstructure of the vertical cross-section of at $\theta = 0^\circ$ (a), (d), 45° (b), (e) and 90° (c), (f). (a)–(c) at low magnification, (d)-(f) at high magnification. (g) Average thickness of the layer of the duplex-like region and the γ bands at $\theta = 0^\circ$. (h) Average grain size in the duplex-like region and the γ bands at $\theta = 0^\circ$. In the duplex-like region, the lamellar and γ grains were taken into consideration on the evaluation of the grain size.

in comparison to those prepared by some conventional processes [26,27] and almost the same as those in the as-EBM components prepared by Hernandez et al. [12].

The γ phase grains in the γ bands at $\theta = 0^\circ$ were observed by TEM, as shown in Fig. 4. The bright-field image was taken with [110] beam direction, as shown in the diffraction pattern. Cracks and pile-up dislocations are hardly observed in the γ grain, though there exists some dislocations with low density. Note that neither cracks nor pile-up dislocations were observed at the interface between the duplex-like region and the γ bands, though the results are not shown here. This reveals that the process parameters of EBM in the present study are suitable for the preparation of Ti-48Al-2Cr-2Nb alloy specimens with high reliability.

On the other hand, it was confirmed by TEM observations that the duplex-like region is composed of fine lamellar γ/α_2 fine grains and fine equiaxed γ grains. Fig. 5(a) and (b) show the bright-field and dark-field images of a lamellar grain in the duplex-like region, respectively. The dark-field image in (b) was taken with the super-lattice diffraction spot of the α_2 phase. The γ and α_2 phases in the lamellar grains are confirmed to satisfy the following orientation relationship as generally reported,

$$\{111\}_\gamma // (0001)_{\alpha 2},\ <110>_\gamma // <11\bar{2}0>_{\alpha 2} \quad (1)$$

The volume fraction of the α_2 phase appears to be small (Fig. 5(b)). The distribution of lamellar thickness was measured using these TEM images and the results are shown in Fig. 5(c) and (d). As shown in these figures, the average thickness of the γ and α_2 lamellae in the lamellar grains are 162 nm and 48 nm, respectively. These values are smaller than those of Ti-48Al polysynthetically twinned (PST) crystals [28,29] and almost identical to those of TiAl alloys fabricated by SLM [16]. These features might depend strongly on the process parameters [16]. All these observations demonstrate that the development of a unique layered microstructure which is hardly obtained by any other processes could be achieved by the present EBM process. The orientation dependence of the deformation behavior of the as-EBM alloys derived from this layered microstructure is described in the next section.;1;

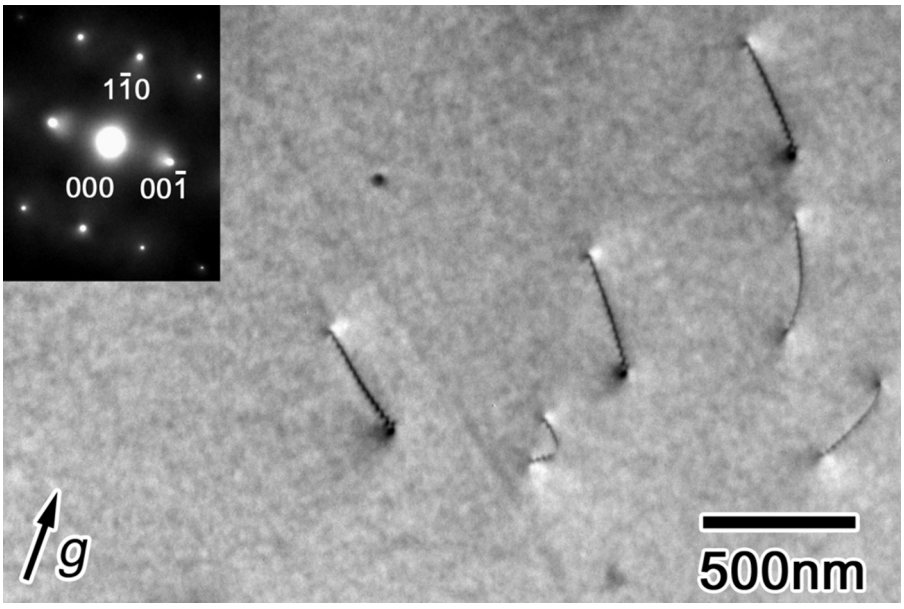

Fig. 4. A bright-filed TEM image of the γ grain in the γ band at $\theta = 0^\circ$; beam direction parallel to [110] direction as shown in the diffraction pattern in the figure.

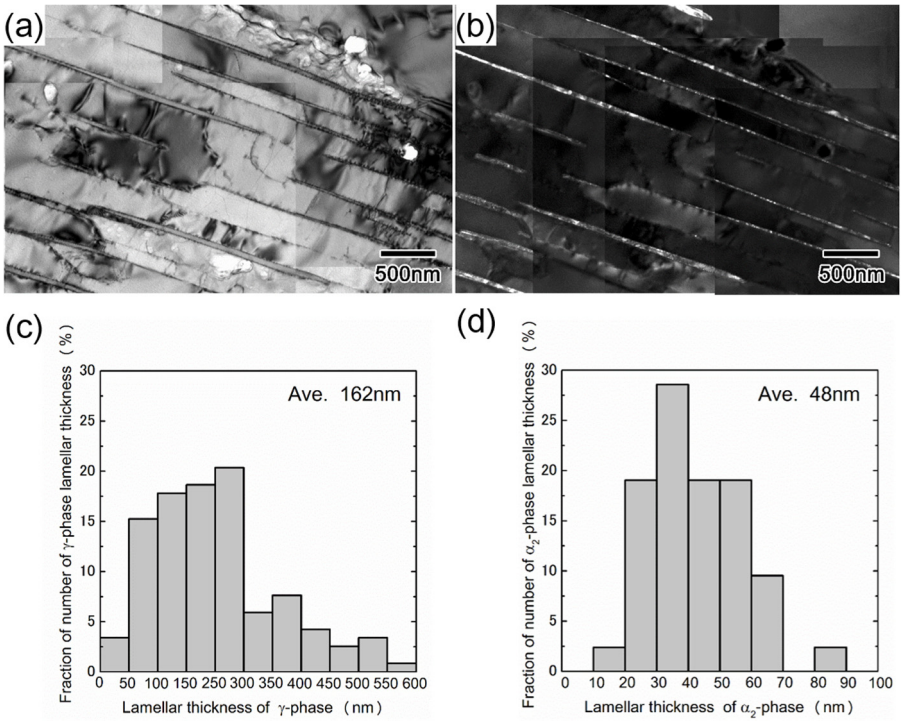

Fig. 5. Bright-field (a) and dark-field (b) images of the lamellar microstructure in the duplex-like region at $\theta = 0^\circ$. Note that the dark-field image was taken with $\boldsymbol{g} = 0001$ of the α_2 phase. Distribution of the thickness of the γ (c) and α_2 (d) phases of the lamellar structure in the duplex-like region at $\theta = 0^\circ$.

3.2. Tensile deformation behavior of EBM-fabricated Ti-48Al-2Cr-2Nb alloy with unique layered microstructure

Tensile tests were conducted to clarify the effect of the unique layered microstructure composed of the duplex-like region and γ bands on the mechanical properties of Ti-48Al-2Cr-2Nb alloy manufactured by EBM. Fig. 6(a) shows the orientation dependence of the tensile stress-strain (S-S) curves at various temperatures. Here, θ is defined to be the angle between the loading axis and the building direction in the alloys. Focusing on the microstructural features described in the previous section, the θ approximately corresponds to the angle between the loading axis and the normal direction of the interface of the layers microstructure in the alloys, as schematically drawn in Fig. 6(a). For all the examined specimens, the S–S curves exhibited a smooth shape. After yielding, strain hardening is observed and the rate of strain hardening gradually decreases when the temperature increases, as shown in Fig. 6(a). At 800 °C, the flow stress tends to decrease with an increase in strain due to necking at any θ. It should be noted that the angle θ has an influence on the yield strength and the tensile elongation of the specimens, especially at room temperature (Fig. 6(b) and (c)). For instance, the yield strength at $\theta = 45^\circ$ was ~566 MPa, which was

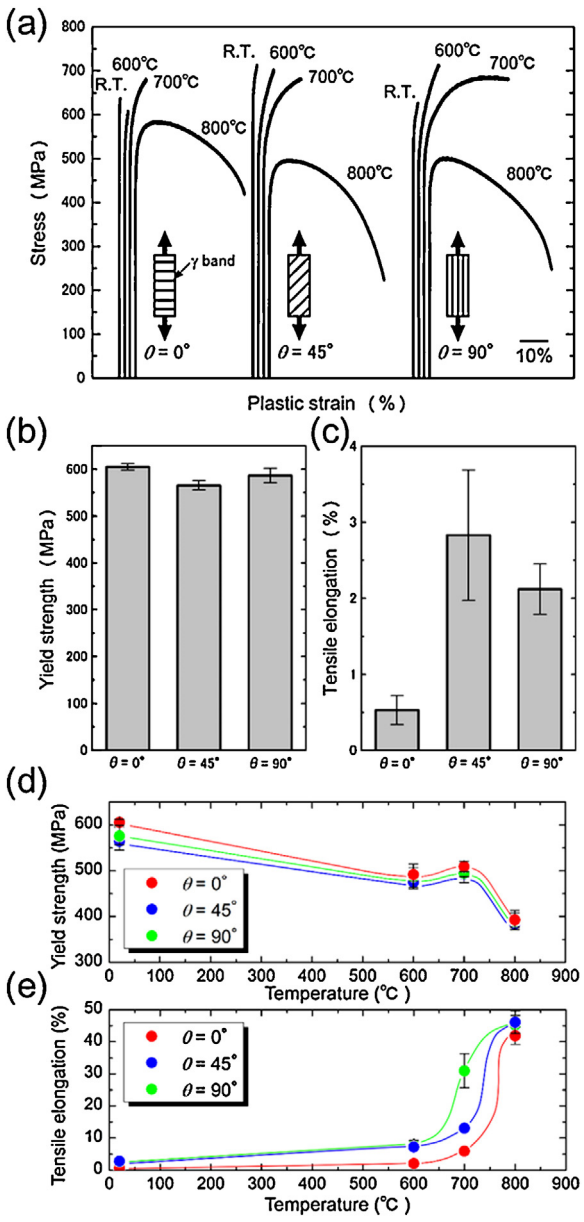

Fig. 6. (a) Tensile stress–strain curves of as-EBM alloy deformed with $\theta = 0^\circ$, 45° and 90° at different temperatures. Variation in the yield strength (b) and tensile elongation (c) of the specimens deformed with $\theta = 0^\circ$, 45° and 90° at room temperature. Temperature dependence of yield strength (d) and tensile elongation (e) of the specimens deformed at $\theta = 0^\circ$, 45° and 90°.

slightly lower than that at $\theta = 0^\circ$ (~605 MPa) and 90° (~587 MPa) at room temperature. However, even at $\theta = 45^\circ$, the yield strength of the as-EBM specimens at room temperature was higher than that prepared by casting [1], owing to the development of much finer microstructure. In addition, the room temperature ductility of the specimen at $\theta = 45^\circ$ is significantly improved to more than 2%, as shown in Fig. 6(c), which significantly quite higher than that for conventional casting [1,3]. On the other hand, the tensile elongation with $\theta = 0^\circ$ and 90° at ambient temperature demonstrates low values, compared with that at $\theta = 45^\circ$. Note that the obtained yield strength and room temperature ductility were larger than those in the Ti-48Al-2Cr-2Nb alloys with non-layered equiaxed microstructure prepared by EBM and following HIP treatment [11]. This also suggests the potential of this material with the layered microstructure in terms of developing structural applications in the future.

Fig. 6(d) and (e) show the temperature dependence of yield strength and tensile elongation at $\theta = 0^\circ$, 45° and 90°. The error bars in this figure correspond to the standard deviation of the values, though the bars smaller than the diameter of the plotted point are not shown. At any θ tested, the yield strength gradually decreases with increasing temperature up to 600 °C followed by an increase in strength (Fig. 6(d)). After showing a peak at 700 °C, the yield strength decreases again as temperature rises. This means that an anomalous strengthening, typical in some intermetallic compounds as the details are discussed later, appears in the as-EBM alloy. It is noted that the yield strength is over 350 MPa even at 800 °C, and the anisotropy of yield strength observed at low temperatures becomes small at 800 °C.

On the tensile elongation of these specimens, it slightly increases with an increase in temperature and significantly rises above 700 °C (Fig. 6(e)). The cracks often forms on the layer interface between the duplex-like region and γ bands. The elongation at $\theta = 0^\circ$ was the lowest at the examined temperatures because this interface arranges perpendicular direction from loading axis. However, the tensile elongation of all the specimens was over 40% at 800 °C and this value is similar to that of Ti-48Al-2Cr-2Nb alloys produced by other processes [1,3].

3.3. Deformation microstructure of Ti-48Al-2Cr-2Nb alloy fabricated by EBM

Fig. 7 shows optical micrographs of the specimens side view after the tensile tests at room temperature. The slip trace and surface relief of deformation twinning can clearly be observed in the γ bands, especially at $\theta = 45^\circ$. This strongly suggests that γ bands act as effective ductile components in the as-EBM alloy. In order to examine the deformation behavior of the γ bands at room temperature, the deformation microstructure was observed by TEM, as shown in Fig. 8. It should be noted that deformation of the γ-phase is known to be controlled by the {111} (a/2)< 1 $\bar{1}$ 0]] ordinary dislocation, {111}a<1 0 $\bar{1}$]] superlattice dislocation and {111} (a/6)<11 $\bar{2}$]] twinning systems [3]. After tensile deformation to fracture with $\theta = 0^\circ$ at room temperature, numerous dislocations are observed in the γ bands. The Burgers vector of the dislocations observed after the tensile deformation was determined by $\boldsymbol{g}\cdot\boldsymbol{b}$ contrast analysis on the bright-field TEM images with several different reflection vectors ($\boldsymbol{g}$ vectors). Both tangled and straight dislocations aligned parallel to [1 1 0] are observed in the γ bands in Fig. 8(b). In contrast, the former is visible with $\boldsymbol{g} = 0\bar{2}0$ (b), $[1\ \bar{1}\ \bar{1}]$ (c, d) and is out of contrast with $\boldsymbol{g} = [\bar{1}\ \bar{1}\ 1]$ (a) and $[\bar{2}\ \bar{2}\ 0]$ (e). On the other hand, straight dislocations show a strong contrast with $\boldsymbol{g} = [\bar{1}\ \bar{1}\ 1]$(a), $0\ \bar{2}\ 0$ (b) and $[\bar{2}\ \bar{2}\ 0]$ (e) while they cannot be seen with $\boldsymbol{g} = [1\ 1\ \bar{1}]$(c, d). From these results, the tangled and straight dislocations are determined to (a/2) $[1\ \bar{1}\ 0]$ and (a/2) [110] ordinary dislocations, respectively. Therefore, the ordinary dislocations preferentially operate in the γ bands in addition to {111} (a/6)< $[1\ 1\ \bar{2}]$] twins at room temperature. It was reported that an activation of these slip and twinning systems strongly depends on the Al concentration [30]. These results are consistent with a previous study showing that the ordinary dislocations and deformation twins move more easily than the superlattice dislocations in Ti-rich TiAl alloys [30].

4. Discussion

4.1. Formation mechanism of the unique layered microstructure composed of the duplex-like region and the γ bands

Ti-48Al-2Cr-2Nb alloy fabricated by EBM in the present study exhibited a unique layered microstructure composed of duplex-like

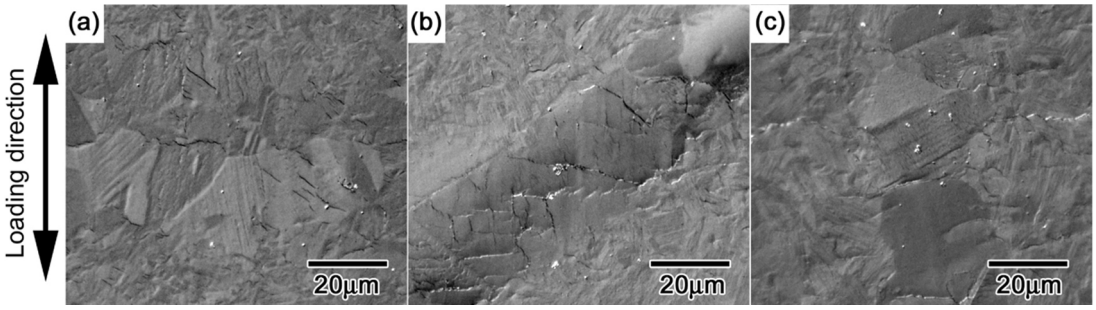

Fig. 7. Side-view images of the specimens tensile deformed to fracture with $\theta = 0^\circ$ (a), 45° (b) and 90° (c) at room temperature.

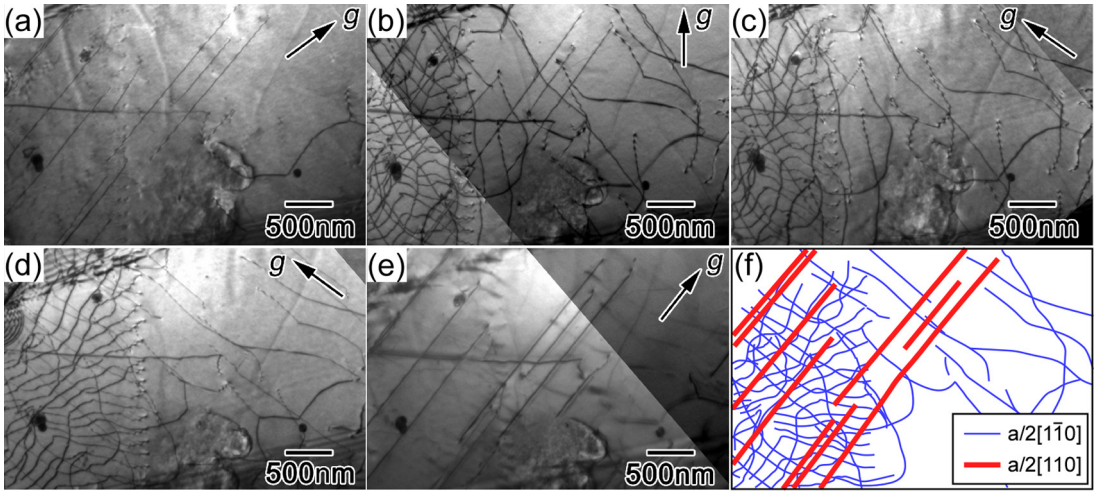

Fig. 8. Bright-field TEM images of dislocation structure in the specimen tensile deformed to fracture with $\theta = 0^\circ$ at room temperature. (a) Beam direction $\boldsymbol{B}//[\bar{1}\ 0\ \bar{1}]$, $\boldsymbol{g} = \bar{1}\ \bar{1}\ 1$, (b) $\boldsymbol{B}//[\bar{1}\ 0\ \bar{1}]$, $\boldsymbol{g} = 0\ \bar{2}\ 0$, (c) $\boldsymbol{B}//[\bar{1}\ 0\ \bar{1}]$, $\boldsymbol{g} = \bar{1}\ \bar{1}\ 1$, (d) $\boldsymbol{B}//[\bar{1}\ 1\ \bar{2}]$, $\boldsymbol{g} = \bar{1}\ \bar{1}\ 1$ and (e) $\boldsymbol{B}//[\bar{1}\ 1\ \bar{2}]$, $\boldsymbol{g} = \bar{2}\ \bar{2}\ 0$. (f) A schematic drawing showing the Burgers vector of dislocations observed in the γ-TiAl grain.

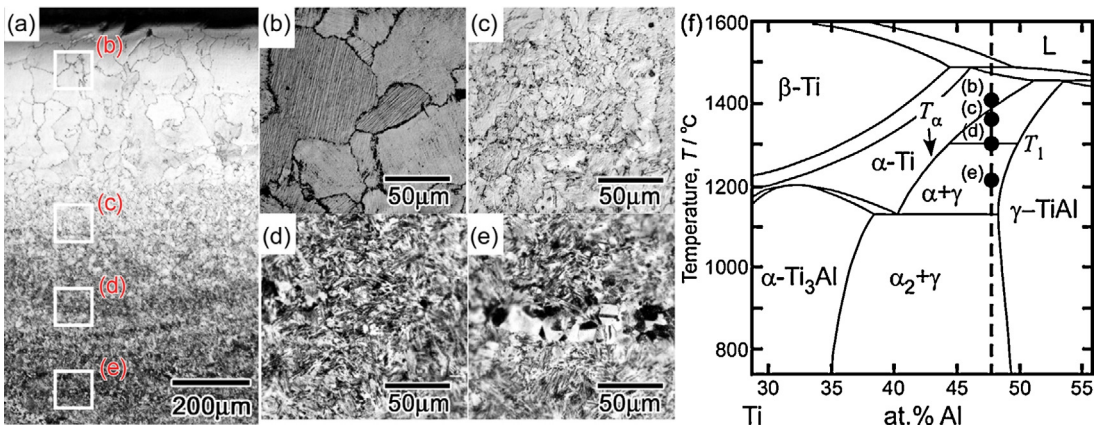

Fig. 9. (a) Microstructure of the last several layers near the top surface built at $\theta = 0^\circ$. (b)–(e) High-magnification images corresponding to the white square regions in (a). (f) Central portion of the Ti–Al phase diagram.

region and γ bands (Fig. 3). The development of similar microstructures were previously reported by Loeber et al. [15] and Terner et al. [31] in Ti-(46-48)Al-2Cr-2Nb and Ti-(47-48)Al-2Cr-8Nb EBM alloys, although the term "layer" was not mentioned. In comparison, "layered" microstructure seems more clearly developed in the present material. In order to understand the formation mechanism of the unique layered microstructure, we observed the last several melting layers close to the top surface of the cylindrical bars at $\theta = 0^\circ$, as shown in Fig. 9(a). The microstructure of the as-EBM specimen varies gradually with increasing distance from the top surface. Fig. 9(b)–(e) show high-magnification micrographs of the white square regions in Fig. 9(a). It is interesting to note that full-lamellar, near-lamellar, duplex-like and near-γ (equiaxed γ) structures can be seen in Fig. 9(b)–(e), respectively. In Fig. 9(e), one can observe the layered microstructure composed of the duplex-like region and the γ bands. It is well known that microstructure of Ti-rich TiAl alloys composed of γ and α_2 phases depends on annealing temperature, as shown in Fig. 9(f). If annealing temperature (T_1) is set to (b), (c), (d) and (e) in the Ti-Al binary phase diagram, full-lamellar, near-lamellar, duplex and near-γ structures are formed,

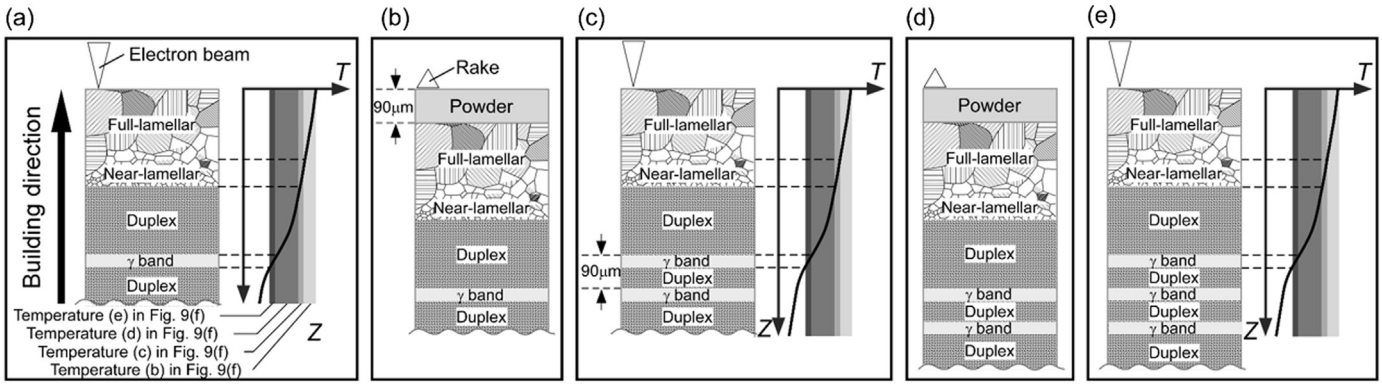

Fig. 10. Schematic illustrations showing the microstructure evolution and the unique layered microstructure formation during the EBM process. (a) a snapshot during the EBM process, (b) feed a powder layer, (c) fusion several layers, (d) feed the next layer and (e) fusion several layers again.

respectively [1–3,32]. The full-lamellar structure which has coarse lamellar grains with alternating stacking of γ and α/α_2 lamellae is formed by heat treatment at temperatures above the α transus (T_α) [1,32]. On the other hand, the near-lamellar structure composed of the many lamellar grains and smaller amount of equiaxed γ grains can be obtained just below T_α. The duplex and near-γ structures are formed in the α + γ region at around 1250 °C and just above the eutectoid temperature, respectively. It should also be noted that the duplex and near-γ structures correspond to the duplex-like region and the γ bands in the as-EBM specimens, respectively. The volume fraction of the α_2 phase decreases with decreasing temperature, resulting in the microstructure change associated with the annealing temperature. During the EBM process, an electron beam locally melts the TiAl alloy powders near the top surface. As a result, the area close to the melting pool is heat treated at different temperatures. It is easily understood that the temperature decreases with increasing distance from the melting pool along the building direction. In this way, the microstructure changed from the top surface in the following sequence: full-lamellar, near-lamellar, duplex-like and near-γ structures, as shown in Fig. 9. Fig. 10 schematically shows the the microstructure evolution during the EBM process. During the process, feed and fusion of the powder layers repeated alternatively. The full-lamellar and near-lamellar regions formed in the vicinity of the top surface are cyclically heat-treated during the EBM process. With increasing powder fusion cycles, the distance between the lamellar regions and the top surface increases. This means that the annealing temperature for the lamellar regions decreases with increasing the number of cycles, and therefore, the regions annealed around 1250 °C changed into the duplex-like region by discontinuous coarsening [33,34]. Finally, the duplex-like region subjected to the heat treatment just above the eutectoid temperature ((e) in Fig. 9(f)) is transformed into the γ bands. Since the pre-heating temperature is 1060 °C, there should be the area annealed at temperatures favorable for the formation of the γ bands, as shown in Fig. 10. In this way, the γ bands perpendicular to the building direction are periodically introduced in the duplex-like region. Note that the microstructure of the area away from the top surface no longer changes. Finally, the unique layered microstructure consisting of the duplex-like region and the γ bands is kept. It should be noted that the sum of the layer thicknesses of the duplex-like region and the γ bands was approximately equal to the thickness of powder layers at each cycle during the EBM process (Fig. 3(g)), which is consistent with the model for the microstructure evolution schematically shown in Fig. 10. The above considerations suggest that the tuning-up of the process parameter in the EBM process is one of the important factors that govern the development of the layered microstructure.

It should however be mentioned that the microstructure is not perfectly layered in the present samples, but a disturbance partly exists. While the major part of the coarser equiaxed γ grains are indeed aligned perpendicularly to the building direction, the layered structure is not perfectly clear and regular at some parts, as it can be seen in Fig. 3. Some duplex structures interrupted the γ bands, and in some zones of several hundreds of microns the deprivation of coarse γ was seen. This suggests that other factors in addition to the process parameters may also affect the formation behavior of the layered microstructure, such as Al evaporation, powder particles size and distribution, and building path strategies. Further investigations must be carried out to clarify this issue.

4.2. Origin of the anisotropic tensile deformation behavior of the EBM-fabricated Ti-48Al-2Cr-2Nb alloy with layered microstructure

Mechanical properties of as-EBM alloy at room temperature exhibited strong plastic anisotropy depending on θ. The as-EBM alloy built at $\theta = 45^\circ$ demonstrated the largest tensile elongation (Fig. 6(c)). This ductility was over 2% and was significantly higher than that of the cast alloys [1]. Not only γ phase is known to show more ductile behavior than α_2 phase, the grain size of the duplex-like region in the layered microstructure was smaller than that of the γ bands, as shown in Fig. 3(h). Thus, the γ bands are expected to be preferentially deformed in as-EBM alloy. In fact, numerous markings of slip/twin traces were concentrated at the γ bands, as shown in Fig. 7. Furthermore, (a/2)<110] ordinary dislocations were frequently observed in the γ bands (Fig. 8). Fig. 11 shows the nanoindentation hardness of the duplex-like region and γ bands at room temperature. The γ bands showed lower hardness than the duplex-like region, as expected. Thus, the duplex-like region acts as the strength component and γ bands act as the ductile component in the as-EBM alloy at ambient temperature. If tensile load is applied to the tensile specimens, a maximum shear stress is achieved at 45° to the loading axis. Therefore, at $\theta = 45^\circ$, shear deformation preferentially took place parallel to the soft γ bands, resulting in large tensile elongation. On the other hand, shear deformation was suppressed by the boundaries between the hard duplex-like region and soft γ bands at $\theta = 0^\circ$ and 90°, which led to low tensile elongation. When the value of elongation was compared in them, it is slightly larger at 90° than that at 0°. This is considered to be related to the different orientation of the cracks propagation path in them, as the details are described later. It is also noted that as-EBM alloy at any θ exhibited higher yield strength at room temperature than the alloys prepared by some other processes [1,11], as shown in Fig. 6(b). Smaller grain size (Fig. 3(h)) and lamellar thickness (Fig. 5(c) and

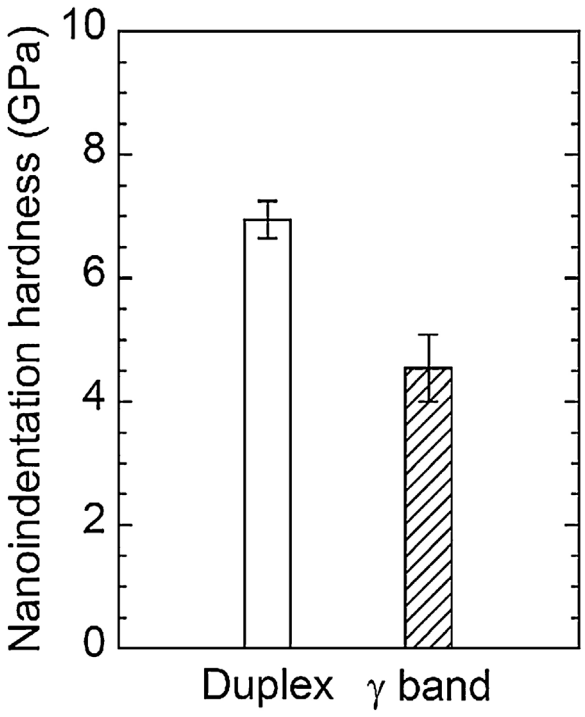

Fig. 11. Nanoindentation hardness of the duplex-like region and the γ bands in as-EBM alloy.

(d)) in the layered microstructure of the as-EBM alloy led to higher yield strength at room temperature.

Plastic anisotropy of the yield strength shown in the as-EBM alloy at room temperature became small at high temperatures, and the tensile elongation rose rapidly above 700 °C (Fig. 6(d) and (e)). It is known that the duplex structure in TiAl alloys is more easily deformed by increasing activity of the slip and twinning systems [11]. Thus, it is considered that the softening of the duplex-like region led to small anisotropy of the yield strength depending on θ. A brittle-to-ductile transition temperature (BDTT) of the duplex-like region existed at around 750 °C, which is slightly lower than the BDTT of this alloy produced by EBM in a previous study [11]. Note that the experimental results shown in Fig. 6(e) demonstrated that the BDTT at 90° is shifted towards a lower temperature compared to both 0° and 45° loading orientations at around the BDTT, although large elongation more than 40% can be obtained in all the specimens above 800 °C. A possible reason for this is the different orientation of the cracks propagation path, which follows the duplex-like and γ bands layers interface, with respect to the loading axis. In the 90° specimen, the propagation of the cracks along the interface of the layered microstructure does not directly lead to the fracture of the specimens, unlike in 0° and 45° specimens. Further study is required to support this assumption.

It is also noted that the anomalous increase in yield strength with increasing in temperature was observed to take place in the as-EBM alloy, as shown in Fig. 6(d). The positive temperature dependence of yield strength was also reported to occur in Ti-rich TiAl alloys [11,35]. This is considered to be induced by the occurrence of yield strength anomaly by $\{1121\}<1\,1\,\bar{2}\,\bar{6}>$ pyramidal slip in the α_2 phase [35], and $\{111\}<1\;\;0\;\;\bar{1}]$ superlattice slip and $\{111\}<1\;\bar{1}\;0\;\;]$ ordinary slip in the γ phase [36–38]. Anomalous strengthening of the as-EBM alloy is favorable for its practical use at high temperatures.

The results obtained in the present study suggest that EBM can develop a unique layered microstructure which is not obtained by any other processes, and thus it has a great potential in terms of developing structural applications for TiAl-based alloys because both high strength and room temperature ductility were achieved in as-EBM TiAl alloy. Since γ-TiAl alloys are considered for high temperature applications, high temerature creep properties are also critical. As described in introduction, the development of a fine microstructure is preferable for improving the ductility and strength, as it was confirmed in this study, while it is generally known to worsen the creep properties. Thus, further optimization of microstructure for ensuring not only the ductility and strength, but also the creep resistance at a high level is essential. The effect of the unique microstructure obtained by EBM on the creep properties of such materials are being presently studied.

5. Conclusions

The microstructure and tensile deformation properties of Ti-48Al-2Cr-2Nb alloy fabricated by EBM were examined, focusing on the development of a unique layered microstructure. The results obtained are summarized and the following conclusions were reached:

1. EBM accompanied by the repeated local heat treatment in the vicinity around the melting pool led to the production of a unique layered microstructure composed of duplex-like regions and γ bands. The γ bands were arranged perpendicular to the building direction.
2. The yield strength and tensile elongation of Ti-48Al-2Cr-2Nb alloy prepared by EBM varied significantly depending on the angle θ between the building direction and the loading direction. At room temperature, the yield strength exhibited high values more than 550 MPa at any θ. The tensile elongation at $\theta = 45°$ was higher than that at $\theta = 0°$ or 90°, and tensile elongation above 2% could be obtained at $\theta = 45°$, owing to the localized shear deformation in the γ bands of the unique layered microstructure.
3. The anisotropy of the yield strength shown in the as-EBM alloy decreased with increasing temperature. The yield strength exhibited a peak at 700 °C, and then decreased above this temperature. All the examined specimens exhibited high yield strength above 350 MPa and good ductility over 40% at 800 °C. These properties are comparable to those of Ti-48Al-2Cr-2Nb alloys produced by other processes.

Acknowledgement

This study was supported by the Cross-Ministerial Strategic Innovation Promotion program (SIP) "Structural Materials for Innovation" from the Japan Science and Technology Agency (JST).

References

[1] Y.-W. Kim, Ordered intermetallic alloys, part III: gamma titanium aluminides, JOM 46 (1994) 30–39.
[2] Y.-W. Kim, D.M., Dimiduk, M.H. Loretto, Gamma Titanium Aluminides 1999, The Minerals Metals & Materials society (TMS), Warrendale, PA, (1999).
[3] F. Appel, J.D.H. Paul, M. Oehring, Gamma Titanium Aluminide Alloys, Wiley-VCH, Singapore, 2011.
[4] X. Wu, Review of alloy and process development of TiAl alloys, Intermetallics 14 (2006) 1114–1122.
[5] M. Yamaguchi, H. Inui, K. Ito, High-temperature structural intermetallics, Acta Mater. 48 (2000) 307–322.
[6] L.E. Murr, Metallurgy of additive manufacturing: examples from electron beam melting, Add. Manu. 5 (2015) 40–53.
[7] L.E. Murr, E. Martinez, K.N. Amato, S.M. Gaytan, J. Hernandez, D.A. Ramirez, P.W. Shindo, F. Medina, R.B. Wicker, Fabrication of metal and alloy components by additive manufacturing: example of 3D materials science, J. Mater. Res. Technol. 1 (2012) 42–54.
[8] D. Cormier, O. Harrysson, T. Mahale, H. West, Freeform fabrication of titanium aluminide via electron beam melting using prealloyed and blended powders, Res. Lett. Mater. Sci. (2007), 34737.

[9] L.E. Murr, S.M. Gaytan, A. Ceylan, E. Martinez, J.L. Martinez, D.H. Hernandez, B.I. Machado, D.A. Ramirez, F. Medina, S. Collins, R.B. Wicker, Characterization of titanium aluminide alloy components fabricated by additive manufacturing using electron beam melting, Acta Mater. 58 (2010) 1887–1894.
[10] J. Schwerdtfeger, C. Körner, Selective electron beam melting of Ti-48Al-2Nb-2Cr: microstructure and aluminium loss, Intermetallics 49 (2014) 29–35.
[11] S. Biamino, A. Penna, U. Ackelid, S. Sabbadini, O. Tassa, P. Fino, M. Pavese, P. Gennaro, C. Badini, Electron beam melting of Ti-48Al-2Cr-2Nb Alloy: microstructure and mechanical properties investigation, Intermetallics 19 (2011) 776–781.
[12] J. Hernandez, L.E. Murr, S.M. Gaytan, E. Martinez, F. Medina, R.B. Wicker, Microstructures for two-phase gamma titanium aluminide fabricated by electron beam melting, Metallogr. Microstruct. Anal. 1 (2012) 14–27.
[13] H.P. Tang, G.Y. Yang, W.P. Jia, W.W. He, S.L. Lu, M. Qian, Additive manufacturing of a high niobium-containing titanium aluminide alloy by selective electron beam melting, Mater. Sci. Eng. A 636 (2015) 103–107.
[14] W. Li, J. Liu, S. Wen, Q. Wei, C. Yan, Y. Shi, Crystal orientation, crystallographic texture and phase evolution in the Ti-45Al-2Cr-5Nb alloy processed by selective laser melting, Mater. Charact. 113 (2016) 125–133.
[15] L. Loeber, S. Biamino, U. Ackelid, S. Sabbadini, P. Epicoco, P. Fino, J. Eckert, (2011). Comparison of selective laser and electron beam melted titanium aluminides, International Symposium, 22nd Solid Freeform Fabrication 547–556.
[16] D. Srivastava, I.T.H. Chang, M.H. Loretto, The effect of process parameters and heat treatment on the microstructure of direct laser fabricated TiAl alloy samples, Intermetallics 9 (2001) 1003–1013.
[17] A.A. Antonysamy, J. Meyer, P.B. Prangnell, Effect of build geometry on the (-grain structure and texture in additive manufacture of Ti-6Al-4 V by selective electron beam melting, Mater. Charact. 84 (2013) 153–168.
[18] X. Tan, Y. Kok, Y.J. Tan, M. Descoins, D. Mangelinck, S.B. Tor, K.F. Leong, C.K. Chua, Graded microstructure and mechanical properties of additive manufactured Ti-6Al-4V via electron beam melting, Acta Mater. 97 (2015) 1–16.
[19] M. Jamshidinia, M.M. Atabaki, M. Zahiri, S. Kelly, A. Sadek, R. Kovacevic, Microstructural modification of Ti-6Al-4 V by using an in-situ printed heat sink in electron beam melting® (EBM), J. Mater. Proc. Technol. 226 (2015) 264–271.
[20] I. Yadroitsev, P. Krakhmalev, I. Yadroitsava, S. Johansson, I. Smurov, Energy input effect on morphology and microstructure of selective laser melting single track from metallic powder, J. Mater. Proc. Technol. 213 (2013) 606–613.
[21] K. Kunze, T. Etter, J. Grässlin, V. Shklover, Texture, anisotropy in microstructure and mechanical properties of IN738LC alloy processed by selective laser melting (SLM), Mater. Sci. Eng. A 620 (2015) 213–222.
[22] S.-H. Sun, Y. Koizumi, S. Kurosu, Y.-P. Li, A. Chiba, Phase and grain size inhomogeneity and their influences on creep behavior of Co-Cr-Mo alloy additive manufactured by electron beam melting, Acta Mater. 86 (2015) 305–318.
[23] V.A.C. Haanapplel, H. Clemens, M.F. Stroosnijder, The high temperature oxidation behavior of high and low alloyed TiAl-based intermetallics, Intermetallics 10 (2002) 293–305.
[24] E.A. Loria, Gamma titanium aluminides as prospective structural materials, Intermetallics 8 (2000) 1339–1345.
[25] M. Lamirand, J.L. Bonnentien, G. Ferrière, S. Guérin, J.P. Chevalier, Effects of interstitial oxygen on microstructure and mechanical properties of Ti-48Al-2Cr-2Nb with fully lamellar and duplex microstructures, Metall. Mater. Trans. A 37 (2006) 2369–2378.
[26] J.N. Wang, J. Yang, Y. Wang, Grain refinement of a Ti-47Al-8Nb-2Cr alloy through heat treatments, Scr. Mater. 52 (2005) 329–334.
[27] H. Clemens, A. Bartels, S. Bystrzanowski, H. Chladil, H. Leitner, G. Dehm, R. Gerling, F.P. Schimansky, Grain refinement in γ-TiAl-based alloys by solid state phase transformations, Intermetallics 14 (2006) 1380–1385.
[28] T.A. Parthasarathy, M.G. Mendiratta, D.M. Dimiduk, Flow behavior of PST and fully lamellar polycrystals of Ti-48Al in the microstrain regime, Acta Mater. 46 (1998) 4005–4016.
[29] H.Y. Kim, K. Maruyama, Stability of lamellar microstructure of hard orientated PST crystal of TiAl Alloy, Acta Mater. 51 (2003) 2191–2204.
[30] T. Nakano, K. Matsumoto, T. Seno, K. Oma, Y. Umakoshi, Effect of chemical ordering on the deformation made of Al-rich Ti-Al single crystals, Philos. Mag. A 74 (1996) 251–268.
[31] M. Terner, S. Biamino, P. Epicoco, A. Penna, O. Hedin, S. Sabbadini, P. Fino, M. Pavese, U.L.F. Ackelid, P. Gennaro, F. Pelissero, C. Badini, Electron beam melting of high niobium containing TiAl alloy: feasibility investigation, Steel Res. Int. 83 (2012) 943–949.
[32] D.M. Dimiduk, D.B. Miracle, Y.W. Kim, M.G. Mendiratta, Recent progress on intermetallic alloys for advanced aerospace systems, ISIJ Int. 31 (1991) 1223–1234.
[33] A. Denquin, S. Naka, Phase transformation mechanisms involved in two-phase TiAl-based alloys-II. Discontinuous coarsening and massive-type transformation, Acta Mater. 44 (1996) 353–365.
[34] J. Yang, J.N. Wang, Y. Wang, Q. Xia, Refining grain size of a TiAl alloy by cyclic heat treatment through discontinuous coarsening, Intermetallics 11 (2003) 971–974.
[35] Y. Umakoshi, T. Nakano, Plastic behaviour of TiAl crystals containing a single set of lamellae at high temperatures, ISIJ Int. 32 (1992) 1339–1347.
[36] T. Kawabata, T. Nakai, O. Izumi, Positive temperature dependence of the yield stress in TiAl $L1_0$ type superrattice intermetallic compound single crystals at 293–1273 K, Acta. Metall. 33 (1985) 1355–1366.
[37] H. Inui, M. Matsumoto, D.-H. Wu, M. Yamaguchi, Temperature dependence of yield stress, deformation mode and deformation structure in single crystals of TiAl (Ti-56at.%Al), Philos. Mag. A 75 (1997) 395–423.
[38] T. Nakano, K. Hagihara, T. Seno, N. Sumida, M. Yamamoto, Y. Umakoshi, Stress anomaly in Al-rich TiAl single crystals deformed by the motion of 1/2<110] ordinary dislocations, Philos. Mag. Lett. 78 (1998) 385–391.